I&EC research
Industrial & Engineering Chemistry Research

Article

pubs.acs.org/IECR

Energy-Optimal Control of RO Desalination

Larry Gao, Anditya Rahardianto, Han Gu, Panagiotis D. Christofides,* and Yoram Cohen*

Water Technology Research Center, Department of Chemical and Biomolecular Engineering, University of California, Los Angeles, California 90095-1592, United States

ABSTRACT: A novel model-based control system for the operation of a spiral-wound RO membrane desalination system was developed with a focus on maintaining energy-optimal operation. The control scheme utilized an operational model for spiral-wound RO desalting with a supervisory controller providing real-time updates of membrane permeability and the appropriate feed pressure set-points for maintaining the target permeate productivity at the lowest feasible specific energy consumption. System RO feed pressure and flow rates were controlled by a lower-level RO controller through adjustment of the RO high pressure feed pump, variable frequency drive, and RO concentrate valve. Seawater desalination tests with an RO plant, capable of permeate productivity up to 18 000 gallons/day, demonstrated effective self-adaptive energy-optimal operation, subject to feed salinity fluctuations, constraints imposed by the system's physical limitations (i.e., minimum and maximum feasible operational pressures and flow rates), and the thermodynamic restriction for cross-flow RO operation.

1. INTRODUCTION

Reverse osmosis (RO) desalination has emerged globally as a leading method for desalting seawater, inland brackish water, and water reuse applications.[1] Since the birth of RO desalination, RO energy consumption has been reduced via the development of membranes of increased permeability,[2−4] more efficient high pressure pumps,[5] optimization of membrane module hydrodynamics,[6−13] and the introduction of energy recovery devices (ERDs).[14,15] ERDs have enabled efficient recovery of unutilized pressure energy from the RO concentrate and have proven particularly effective for large-scale seawater RO plants.[16−18] However, ERDs designed for small RO systems are of low efficiency, are of a relatively high capital cost, and may introduce inflexibility in terms of system control.[19] It is important to recognize that RO operation may be confronted with temporal variability of feedwater quality, as well as by various water production objectives.[20,21] In this regard, effective process control and optimization are important for small RO systems in order to lower the overall cost of permeate water production.[21−24]

RO plant control via classical control algorithms (i.e., proportional−integral (PI) control) has been deployed to control system pressure in order to meet permeate production set-points.[25] Multiloop control of both permeate flow rate and permeate quality have also been proposed.[26] In addition to classical control, several nonlinear model-based control strategies have been developed to improve RO process control under conditions of varying feedwater quality and correct various faults that may occur during operation.[27,28] Model-predictive control (MPC) and Lyapunov-based control have also been designed and evaluated through computer simulations.[28−32] More recently, an RO control strategy that considers minimization of energy consumption has been introduced with the concept demonstrated in a small laboratory RO system.[33] The above study introduced the role of the thermodynamic restriction[34] and specific energy consumption (SEC) in the optimization and control of cross-flow RO operation.

A theoretical framework for minimization of RO permeate production cost was introduced recently,[34−36] within the context of the SEC and thermodynamic restriction,[34] that considered the impact of water recovery, energy recovery and pumping efficiencies, feed and permeate flow rate constraints, membrane module topology,[34−36] and optimization of feed pressure subject to feed salinity fluctuations.[37] An energy optimization nonlinear control algorithm (without the inclusion of an ERD) that builds on the above SEC modeling framework was also demonstrated with a small laboratory spiral-wound RO system. It was shown, in limited proof-of-concept laboratory tests, that energy-optimal control for spiral-wound RO operation, subject to a simple step change in feed salinity, was feasible through simultaneous control of feed pressure and feed flow rate.[33] The above approach provided a framework for a controller architecture that can be deployed for RO operation that is confronted with temporal variability of both RO membrane permeability (e.g., due to membrane fouling or aging) and feedwater salinity.

In the present work, an approach for control of RO plant operation is introduced, following the general scheme in ref 33, demonstrating the integration of lower-level and supervisory controllers. Implementation of the control algorithm only requires operator input of the target permeate production (i.e., RO permeate flow rate set-point). The control system then automatically considers constraints imposed by the required permeate production, system operability (e.g., operational limitation of system components), high pressure feed pump and ERD efficiencies, membrane permeability changes, and temporal variability of feed salinity. The proposed RO controller was field demonstrated for seawater desalination with respect to (a) maintaining pressure and flow rate (feed

Special Issue: John Congalidis Memorial

Received: July 19, 2013
Revised: August 28, 2013
Accepted: September 2, 2013
Published: September 2, 2013

dx.doi.org/10.1021/ie402304d | Ind. Eng. Chem. Res. 2014, 53, 7409−7420

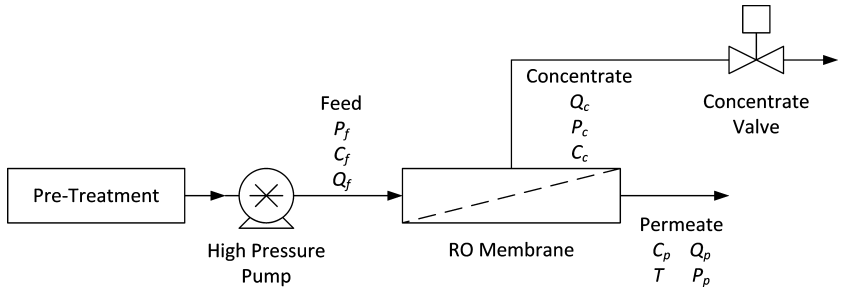

Figure 1. Schematic of the RO desalination process depicting the various monitored process variables.

and permeate streams) set-points and (b) ensuring energy-optimal operation with temporally variable feed salinity.

2. EXPERIMENTAL SECTION

2.1. Desalination System. Energy-optimal control strategy was implemented in a reverse osmosis (RO) seawater desalination system integrated with feed treatment (microfiltration and ultrafiltration). The RO system had a maximum permeate production capacity of 18 000 GPD (68.1 m^3/day) with three 8 in. spiral-wound elements in series (DOW FILTMEC SW30HRLE-400, Dow, Edina, MN). Each element had a manufacturer-recommended maximum operating water recovery of 15%, enabling up to a total recovery of 38.6% for the three elements in series. The RO membrane elements had manufacturer reported rejection of 99.60% (32 000 ppm NaCl at 800 psi or 5.5 MPa). Each of the RO elements was housed in a fiberglass pressure vessel (8 in. end ported, Protec Arisawa PRO-8-1000-EP-1, Vista, CA) with a manufacturer-specified maximum operating pressure of 6.89 MPa (1000 psi).

The RO system (Figure 1) consisted of a high-pressure axial piston positive displacement pump (APP 10.2, Danfoss, Nordborg, Denmark) with a premium efficiency motor (CEM4103T, 25 hp, TEFC, Baldor, Fort Smith, AR) and a variable frequency drive (VFD) system (VLT AQUA Drive FC 202, 22 kW, Danfoss, Nordborg, Denmark). The pump, with measured efficiency of 91.5%, had a manufacturer-specified flow and pressure limits of 66−170 L/min and 2−8 MPa, respectively. The pump VFD, equipped with internal current and voltage sensors, produced electrical consumption as a standard VFD output. The above minimum pump feed flow rate and pressure were required in order to ensure adequate pump self-lubrication. An actuated needle valve (Mark 708LMO, Richard Industries, Cincinnati, OH), installed at the RO concentrate exit, along with the pump VFD, enable control of both the feed pressure and feed flow rate. The desalination pilot was instrumented with an array of sensors for monitoring process variables such as flow rates, pressures, conductivity, and temperature. The primary process variables used for system control included pressures (P_f, P_c, P_p), flow rates (Q_f, Q_c, Q_p), and salinities (C_f, C_c, C_p) of the feed, concentrate, and permeate streams, respectively, in addition to the permeate temperature (T).

2.2. Field study. The RO desalination pilot was deployed at U. S. Naval Base Ventura County (Port Hueneme, CA) with raw seawater feed pumped from an open-sea intake through a screen filter to the feed pretreatment subsystem. The range of feedwater quality over the duration of the field study is listed in Table 1. The feed pretreatment system provided RO feedwater with turbidity $\lesssim$0.1 NTU and enabled fouling-free operation of the RO over the study period. In one specific experiment, the RO system was allowed to foul by reducing the level of feed pretreatment in order to assess the capability of the controller; the change in membrane permeability was tracked and, accordingly, system operation settings self-adapted to maintain energy-optimal operation. Other experiments included evaluation of the system controller performance (i.e., with respect to maintaining permeate productivity and energy-optimal operation), subject to step changes in permeate production set-point and short-term temporal variability of RO feedwater salinity.

Table 1. Feed Water Quality at Port Hueneme, US Naval Base

variable	range
TDS (total dissolved solids)	33 440−36 800 ppm
TSS (total suspended solids)	0.1−5.2 ppm
turbidity	1.7−14 NTU
temperature	11.2−19.7 °C
pH	7.5−8.2

3. CONTROL SYSTEM ARCHITECTURE

The desalination system was operated via a control system (Figure 2) that consisted of a supervisory and low-level RO controllers. The supervisory controller (Figure 3) collects and processes sensor data and performs necessary calculations to establish the operational set-points and trajectories and communicates those to the lower-level RO controllers. During desalting operation, data from system sensors are acquired and passed to the supervisory controller for online calculation of membrane permeability. This controller then uses an energy-optimization algorithm to determine the optimal product water recovery and the corresponding RO feed flow rate set-point for a desired preset RO permeate flow rate. Subsequently, the supervisory RO controller calculates the required RO feed pressure via the RO process model to achieve the desired permeate flow rate set-point. The computed parameters are then communicated to the lower-level RO controller, which controls the RO pump VFD and concentrate valve to attain their specified set-points. The above process is repeated dynamically at a prescribed rate (typically every ∼10−20 s) at a frequency which is set at the supervisory controller level.

3.1. Energy-Optimal Operation. Optimal control of RO desalination requires a framework for predicting energy consumption with considerations of the system physical constraints (e.g., with respect to permeate productivity, feed flow rate, and system pressure) as well as limitations imposed by the thermodynamic restriction in cross-flow operation.[34] In the present work, a generalized framework was adopted for modeling the specific energy consumption (SEC) for RO desalting, defined as the energy expended for producing a unit

dx.doi.org/10.1021/ie402304d | Ind. Eng. Chem. Res. 2014, 53, 7409−7420

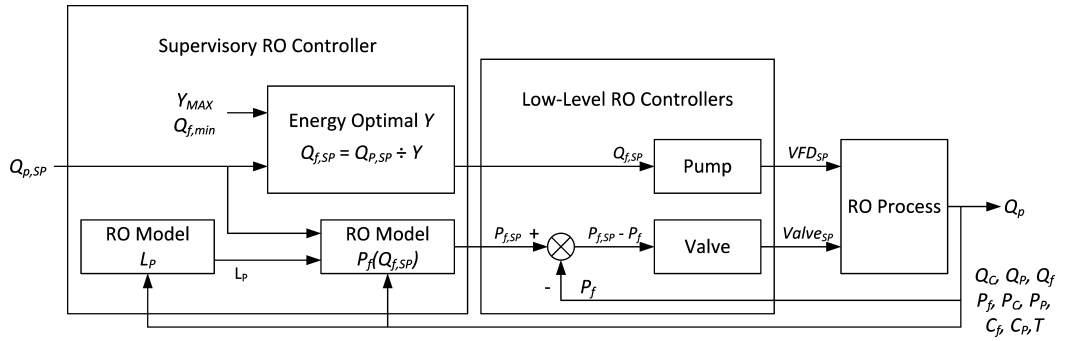

Figure 2. Schematic diagram of the RO system control architecture. The overall control system is separated into a supervisory RO controller and a lower-level RO controller. (Note: Definitions of the monitored process variables are provided in Section 3.1; subscript "sp" denotes a control set-point for the specific variable, L_p is the membrane permeability, Y is the operational water recovery, and VFD_{sp} and $Valve_{sp}$ refer to the set-point settings for these system components).

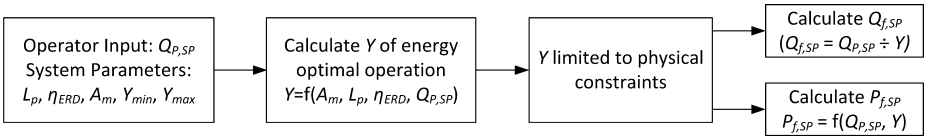

Figure 3. Flowchart of the RO supervisory controller used to calculate $Q_{f,sp}$ and $P_{f,sp}$.

volume of permeate. Accordingly, the optimal SEC (for a given recovery) for a system that can operate up to the limit imposed by the thermodynamic restriction can be expressed as[34]

$$SEC_{norm} = \left[\frac{1 - \eta_{ERD}(1 - Y)}{Y(1 - Y)}\right]\left(\frac{R}{\eta_{pump}}\right) \quad (1)$$

where η_{pump} and η_{ERD} are the pump and ERD efficiencies, respectively, R is the membrane salt rejection, Y is the permeate recovery (i.e., $Y = Q_p/Q_f$), and the normalized SEC_{norm} is defined as $SEC_{norm} = SEC/\pi_o$, where π_o is the RO feed osmotic pressure. When the given RO system is constrained with respect to its permeate production flow rate (Q_p), the SEC is given by[34]

$$SEC_{norm} = \left[\frac{Q_{p,norm}}{Y} - \frac{\ln(1 - Y)}{Y^2}\right] \times [1 - \eta_{ERD}(1 - Y)] \times \left(\frac{R}{\eta_{pump}}\right) \quad (2)$$

where $Q_{p,norm}$ is the normalized permeate flow rate defined as $Q_{p,norm} = Q_p/(A_m L_p \pi_o)$, in which A_m and L_p are the membrane surface area and permeability, respectively. It is noted that for a constrained feed flow rate operation the first term on the right-hand side of eq 2 is replaced by Q_f.[34] Equations 1 and 2 provide a lower limit of SEC with respect to axial pressure drop along the RO element retentate channel and average concentration polarization level by assuming that the effects of both of these factors on SEC are negligible. The relationship between the operational recovery, Y_{min}, at the globally minimum energy consumption for a constrained permeate flow rate, $Q_{p,norm}$, can be obtained by setting $(\partial(SEC_{norm})/\partial Y) = 0$ and solving to obtain the following explicit relationship for $Q_{p,norm}$:

$$Q_{p,norm} = \frac{\ln(1 - Y_{min})[2(1 - \eta_{ERD}) + Y_{min}\eta_{ERD}]}{Y_{min}(1 - \eta_{ERD})} + \frac{1 - \eta_{ERD}(1 - Y_{min})}{(1 - Y_{min})(1 - \eta_{ERD})} \quad (3)$$

Equation 3 is both twice continuously differentiable with respect to Y_{min} and for any given $Q_{p,norm}$ has a single, isolated root for Y_{min} for values of Y_{min} in the domain of $Y = (0,1)$. Therefore, for any given $Q_{p,norm}$, a corresponding Y_{min} can be calculated using Newton's or the secant method. However, it is noted that for a given recovery, RO operation below the SEC_{norm} as set by eq 1 is thermodynamically infeasible.[34] For these cases, the RO system must operate at recovery Y_{tl} where the constant $Q_{p,norm}$ curve intersects the curve representing operation up to the thermodynamic limit (Figure 4). As an

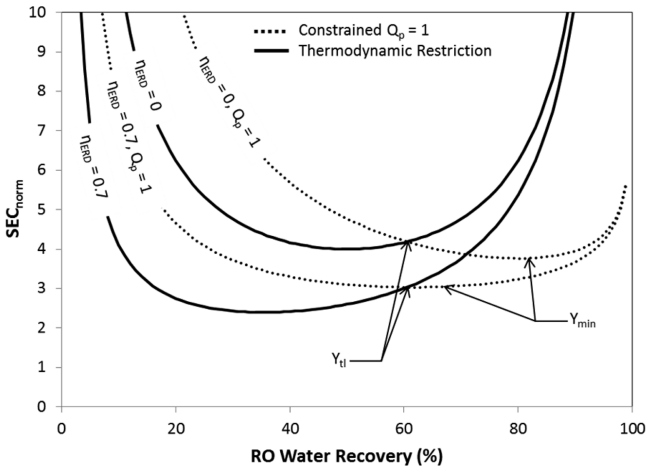

Figure 4. A plot of SEC_{norm} with respect to fractional water recovery, Y, for η_{ERD} values of 0 and 0.7 and $Q_{p,norm}$ of 1. Y_{tl} is the recovery at which the constrained $Q_{p,norm}$ curve intersects the curve representing operation up to the thermodynamic limit, and Y_{min} is the recovery at the globally minimum SEC_{norm} for the case of constrained Q_p.

dx.doi.org/10.1021/ie402304d | Ind. Eng. Chem. Res. 2014, 53, 7409−7420

example, the functional dependencies of SEC_{norm} on recovery for different values of η_{ERD} for operation up to the thermodynamic limit and for cases of constrained permeate flow rate are illustrated in Figure 4 for the case of $\eta_{pump} = 1$, $R = 1$, and $Q_{p,norm} = 1$.

In order to simplify the control algorithm, it is convenient to first identify if Y_{min} would be located above or below the curve representing operation up to the thermodynamic limit (e.g., solid curves in Figure 4). The above can be achieved by noting that Y_{tl}, or the point at which the constant $Q_{p,norm}$ curve intersects with the curve representing operation up to the thermodynamic limit, can be determined by equating eq 1 and eq 2, resulting in

$$Q_{p,norm} = \frac{1}{(1 - Y_{tl})} + \frac{\ln(1 - Y_{tl})}{Y_{tl}} \quad (4)$$

The right-hand side of eq 4 is a strictly increasing function of Y_{tl} over the domain $Y = (0,1)$ with a unique value of Y_{tl} for each $Q_{p,norm}$. It is also noted that as $Y \to 0$, SEC_{norm} for operation with constrained Q_p (eq 2) is greater than SEC_{norm} for operation up to the thermodynamic limit (eq 1); That is,

$$\left[\frac{Q_{p,norm}}{Y} - \frac{\ln(1 - Y)}{Y^2}\right][1 - \eta_{ERD}(1 - Y)] > \frac{1 - \eta_{ERD}(1 - Y)}{Y(1 - Y)} \quad (5)$$

The above inequality can be proven by multiplying it by Y and setting $1 - Y \approx 1$ for the case of $Y \to 0$, which implies that $Q_{p,norm} > 0$. Thus, the inequality holds as $Y \to 0$ for all valid values of $Q_{p,norm}$, which are by definition greater than zero. Because eq 1 and eq 2 have one unique intersection, inequality eq 5 holds true for all values of Y from 0 up to Y_{tl}. This implies that in the region of $Y = (0, Y_{tl}]$, the globally minimum SEC for a constrained Q_p operation exists above the SEC for operation up to the thermodynamic limit. However, for the region of $Y = [Y_{tl},1)$, the globally minimum SEC for a constrained Q_p process exists below the SEC for RO desalting operation up to the thermodynamic limit and, hence, is infeasible. Therefore, the above analysis concludes that if $Y_{min} < Y_{tl}$, then Y_{min} will be the SEC-optimal operating recovery and if $Y_{min} > Y_{tl}$, then Y_{tl} will be the SEC-optimal operating recovery.

3.2. Physical System Constraints. RO desalination plants are not typically designed to operate up to the limit imposed by the thermodynamic restriction. RO plant operation may be constrained by production targets, finite membrane area, and finite membrane permeability, all of which may force operation away from the limit imposed by the thermodynamic restriction. Moreover, physical constraints on system components (i.e., pumps, pressure vessels) can limit the range of RO plant operability (e.g., in terms of the attainable ranges of feed pressure, feed flow rate and permeate recovery). As a result, the optimal RO plant operation as derived in Section 3.1, for a given permeate flow rate, will lead to SEC that is higher relative to the optimal minimum expressed by eq 1. Therefore, optimal operation of the RO system must consider constraints that affect water recovery (Y), product flow rate (Q_p), and feed flow rate (Q_f). The implications of the above, with respect to the SEC, are illustrated in the SEC curves shown in Figure 5 for the RO system used in the present study (Section 2.1). The SEC curves were generated by first determining the permeate flow rate that can be achieved by the present RO system at the maximum and minimum feed pressures and feed flow rates and subsequently calculating the SEC as per eq 2. It is noted that the SEC_{norm} for any of the constrained conditions is above the SEC_{norm} for operation up to the thermodynamic limit. At the minimum system pressure, the SEC_{norm} approaches operation up to the thermodynamic limit; however, such operation is infeasible for the present system due to the minimum Q_f constraint for the physical system. More importantly, the feasible operational domain for the RO system (indicated in the shaded gray area) is bound by the maximum and minimum feed flow rate, maximum feed pressure, and maximum recovery constraints. Between the possible operating $Q_{p,norm}$ of 0.035−0.88 (1.9∼47.3 L/min), Y_{min} is calculated to be 72%∼79%; both values exist above the manufacturer stated Y_{max} of 38.6% (Section 2.1). Hence, within this operating region, while permeate flow rate is constrained, increased recovery would lead to lower SEC_{norm}. Therefore, energy-optimal operation for a constrained permeate flow rate dictates operation at the highest achievable recovery, subject to the constraints imposed by the system. It is noted that for several experiments, more conservative system constraints were implemented instead of values specified by the manufacturer. The specific values used for the constraints in the different experiments are provided in Section 4.

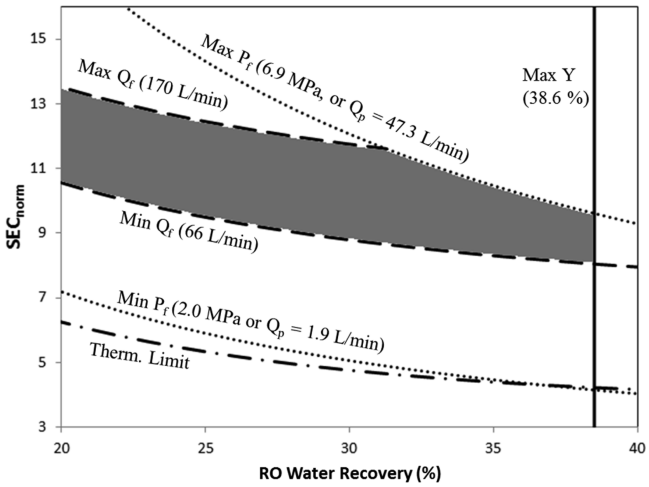

Figure 5. Normalized SEC with respect to RO recovery, with physical plant constraints plotted. Solid lines represent the maximum Y constraint, dashed lines represent the Q_f constraint, the dotted lines represent the Q_p constraint which is governed by the P_f constraint, and the dash-dotted line represents the thermodynamic limit. The operating region of the experimental RO system is shaded.

3.3. RO Feed Pressure Set-Point. In order to operate the RO system at the desired level of permeate productivity but minimize energy consumption, the RO system should be operated at the highest recovery possible under the system physical constraints (Section 2.1). Accordingly, one of the functions of the supervisory controller is to calculate the pressure required to achieve the permeate production set-point making use of the classical permeate flux expression[38]

$$Q_p = A_m L_p (\Delta P_m - \overline{\Delta\pi}) \quad (6)$$

where A_m is the active membrane area, L_p is the membrane hydraulic permeability, ΔP_m is the transmembrane pressure, and $\overline{\Delta\pi}$ is the average osmotic pressure difference across the membrane. Assuming a linear pressure profile along the

dx.doi.org/10.1021/ie402304d | Ind. Eng. Chem. Res. 2014, 53, 7409−7420

retentate channel of the RO elements,[20] the average transmembrane pressure can be expressed as

$$\Delta P_m = \frac{P_f + P_c}{2} - \overline{P}_p \tag{7}$$

where $\overline{P}_p$ is the average permeate-side pressure, P_f is the feed pressure, and P_c is the concentrate pressure at the module exit. The first term on the right-hand side of eq 7 represents the average feed-side pressure. The average feed-side osmotic pressure difference is as follows:[39]

$$\overline{\Delta\pi} = \pi_o \frac{\ln(1-Y)}{Y}\overline{CP} - \pi_o(1-R) \tag{8}$$

where π_o is the feed osmotic pressure, $\overline{CP}$ is the average concentration polarization modulus in each RO membrane element (i.e., $\overline{CP} = C_m/C_b$, where C_b and C_m are the average salt concentrations in the bulk and at the membrane surface, respectively), and R is the observed salt rejection defined as

$$R = 1 - \frac{C_p}{C_f} \tag{9}$$

where C_p and C_f are permeate and feed concentrations, respectively. The feed osmotic pressure can be estimated by:[39]

$$\pi_o = \phi \cdot C_f \cdot (273.15 + T) \tag{10}$$

in which feed concentration (C_f), the osmotic pressure coefficient (ϕ), and temperature (T) are used as a temperature correction factor. The average concentration polarization applicable to the membrane elements used in the present work (Section 2.1) was estimated as[39]

$$\overline{CP} = \exp(0.7[1 - (1-Y)^{1/n}]) \tag{11}$$

in which n is the number of RO membrane elements in series ($n = 3$ for the present system). Combining eqs 6−8 results in the following equation for the permeate flow rate:

$$Q_p = A_m L_p \left[\frac{P_f + P_c}{2} - P_p - \pi_o \frac{\ln(1-Y)}{Y}\overline{CP} + \pi_o(1-R) \right] \tag{12}$$

from which the membrane permeability, L_p, can be initially determined as the system ramps up its operation, given measured values of Q_p and P_f. Subsequently, the permeate production set-point and the calculated permeability are used to calculate the required RO feed pressure P_f. The membrane permeability is calculated and updated dynamically as needed for the calculation of the required feed pressure.

3.4. Lower-Level RO Controller. The supervisory RO controller provides the lower-level RO controller (Figure 2) with the necessary feed pressure and flow rate set-points. The lower-level controller consists of a linear model for the RO pump VFD and a PI controller for the concentrate valve. The lower-level controllers do not enforce decoupling of the two control loops in the closed-loop system; that is, a change in the RO pump VFD setting may affect the RO feed pressure regulated by the RO concentrate valve feedback controller. In this regard, it is stressed that the required feed pressure set-point for optimal operation is determined via a process model (eq 12). However, at the same time, it is important to constrain the VFD ramp speed in order to partially decouple the dynamics of the two control loops and allow the valve controller to provide responsive control on pressure even when the feed flow rate is changing. Although the determination of these time constants of the two control loops can be done a priori on the basis of a process model, in the present work, step tests were used to determine these time constants and the present system's 5 rpm/s VFD ramp speed constraint. It is noted that multivariable control design could be used to provide an integrated approach to control action calculation for both inputs. However, given the significantly different time constants of the two control loops when the VFD ramp speed is constrained, such an approach is not expected to substantially improve the achievable closed-loop performance. At the same time, coupling of the controllers would considerably increase the burden of controller maintenance and decrease the robustness of the overall control architecture.

For the present RO pump/VFD combination (Section 2.1), the linear relationship between the pump RPM (VFD_{sp}^{RO}) and feed flow rate ($Q_f^{desired}$) was determined experimentally as

$$VFD_{SP}^{RO} = \left(11.38 \frac{RPM}{L/min}\right) Q_f^{desired} - 29.009RPM \tag{13}$$

The Q_f set-point is calculated using the energy-optimal Y determined in Sections 3.1, 3.2 and the Q_p set-point as specified by the desired permeate productivity. Given this Q_f set-point as provided by the supervisory controller, eq 13 is then used to determine the required RO VFD setting.

Adjustment of the applied feed pressure is most sensitive to the RO concentrate valve position ($Valve_{sp}$) which was controlled by a PI controller of the following form:

$$Valve_{SP} = K_p^1 (P_{RO,feed}^{SP} - P_{RO,feed}(t)) + \frac{K_p^1}{\tau_i^1}\int_0^t (P_{RO,feed}^{SP} - P_{RO,feed}(\tau))d\tau \tag{14}$$

in which $Valve_{sp}$ is the control action applied to the RO valve, $P_{RO,feed}^{SP}$ is the pressure set-point for the RO feed pressure, K_p^1 is the proportional gain, and τ_i^1 is the integral time constant. Initial experiments carried out over a range of operational parameters enabled tuning of the PI controller parameters to their optimal values of $K_p^1 = -0.0725$ (Valve %/MPa) and $(K_p^1/\tau_i^1) = 0.001$ s.

Due to feed pressure fluctuations caused by the pump (e.g., ±70 KPa in amplitude, or 8% of the feed pressure), tighter control of the pressure cannot be achieved once the set-point tracking error (i.e., absolute difference between the pressure and its set-point) becomes very small (as defined by an upper bound on the error which was set at 70 KPa). Therefore, the use of the PI controller when the tracking error becomes smaller than the upper error bound is counterproductive and would increase sensitivity of the closed-loop system to disturbances due to pump operation. Therefore, in the present control scheme, the PI controller was intermittently deactivated when the difference between the set-point and the pressure was below the upper bound pressure error threshold such that

dx.doi.org/10.1021/ie402304d | Ind. Eng. Chem. Res. 2014, 53, 7409−7420

$$\text{If } |P^{SP}_{RO,feed} - P_{RO,feed}(t)| > 70 \text{ kPa}$$
$$\text{then } K_p^1 = -0.0725\frac{\text{Valve\%}}{\text{MPa}} \text{ and } \frac{K_p^1}{\tau_i^1} = 0.001 \text{ s}$$

$$\text{If } |P^{SP}_{RO,feed} - P_{RO,feed}(t)| < 70 \text{ kPa}$$
$$\text{then } K_p^1 = 0\frac{\text{Valve\%}}{\text{MPa}} \text{ and } \frac{K_p^1}{\tau_i^1} = 0 \text{ s}$$

4. RESULTS AND DISCUSSION

The controller performance under both steady-state and non-steady-state conditions initially focused on establishing the capability for energy-optimal operation under a permeate flow rate set-point of 31.4 L/min with the constraints minimum feed flow rate (Q_f) of 66 L/min, maximum recovery (Y) of 38.6%, and maximum feed pressure (P_f) of 6.9 MPa. The controller was able to maintain the RO permeate flow rate set-point with a deviation of ±0.6% and the target maximum RO water recovery with a deviation of ±0.3%. On the basis of the recorded pump electrical power utilization, system pressures, flow rates, and stream salinities, the pump efficiency was determined to be 91.5 ± 1% and salt rejection was calculated to be 99.6 ± 0.01%. Optimal energy operation was achieved as illustrated in Figure 6, which depicts the SEC curves as described by eq 2. System

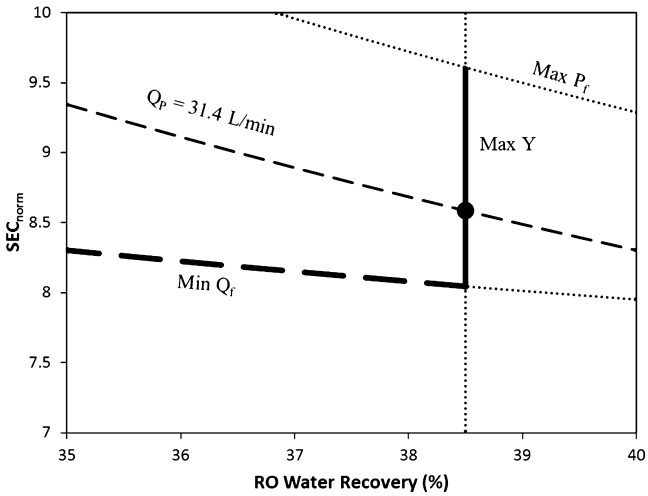

Figure 6. Normalized SEC with respect to RO recovery under the constraints min(Q_f) = 60 L/min, max(P_f) = 6.9 MPa, and max(Y) = 38.6% for the target permeate flow rate set-point (Q_p = 31.4 L/min). The solid circle denotes the plant operating point as established by the controller, which matches the expected theoretical prediction.

operation was along the SEC curve for the permeate flow rate set-point at the maximum possible recovery (and thus lowest energy consumption; see Section 3.2) given the above constraints. Lower energy consumption is possible by operating the system at the minimum possible feed flow rate; however, this would result in a permeate production flow rate that is 22% below the desired set-point.

The controller time response to a permeate flow rate set-point change was subsequently evaluated in an experiment in which the system was first operated at a permeate flow rate set-point of 26.5 L/min. Once steady state was reached, the permeate flow rate set-point was reduced by 14% to 22.7 L/min with the response as shown in Figure 7. For the above operation, system constraints were set as min(Q_f) = 72.7 L/min, max(P_f) = 6.9 MPa, and max(Y) = 30%. The low recovery constraint was chosen to be below the system maximum physical recovery constraint (38.6%) in order to test a wider range of controller operability (i.e., above and below the set-point). As is evident in Figure 7 panels a and b, upon a step change in the target permeate production, the controller drove the system to its new steady state within a short period (~30 s) and maintained the maximum allowable recovery (i.e., for the set recovery constraint).

The controller performance as shown in Figure 7a,b was achieved through the supervisory RO controller that established the new pressure and feed flow rate set-points as 5.07 MPa and 78 L/min, respectively, relative to their previous corresponding values of 5.43 MPa and 90.8 L/min. Subsequently, the lower-level RO controller (Figure 1) drove the system toward steady state with relatively minor oscillations (Figure 7c,d); this was largely because the lower-level controller utilizes a slightly under-damped closed-loop response for both the pump VFD and concentrate valve (Section 3.4). The operating conditions established by the RO controller can be visualized on the SEC plots for the constrained permeate flow rates (before and after the set-point change) as shown in Figure 8. It is clear that the RO system operation, for both permeate flow rate constraints, results in the lowest attainable SEC (corresponding to the highest achievable constrained recovery) as predicted in eq 2.

In order to evaluate the impact of the minimum feed flow rate constraint on the controller's performance, the RO permeate flow rate set-point was reduced by 35%, from 26.5 to 17 L/min. The SEC curves (Figure 9) for the above constrained permeate production (Q_p = 17 L/min) and for operation at the minimum feed flow rate (min(Q_f)) intersect at Y = 23.4%. Clearly, one would have to operate at the highest possible recovery to achieve the lowest SEC for the above constraints, which for the previous example (Figure 8) was constrained to a maximum of 30%. However, in transitioning from the higher to lower permeate flow rate set-points, the SEC curve for min(Q_f) cannot be crossed. In fact, in order to achieve the target permeate productivity, the RO system would have to operate at a recovery where the SEC curves for Q_p = 17 L/min and min(Q_f) = 72.7 L/min intersect. Accordingly, the low-level RO controller adjusted the RO recovery to Y = 23.4% (for the Q_p set-point of 17 L/min) as instructed by the supervisory controller (Figure 10), with steady-state operation for the new set-point achieved within ~30 s.

In order to explore the controller's performance subject to temporal changes in feed salinity, a disturbance in the RO feed salinity was introduced using a high salinity pulse input (Figure 11). This was achieved by mixing RO concentrate with the raw seawater feed to achieve a salinity pulse of ~100 s during which the RO feed salinity peaked up to 17% above the raw seawater feed. Under the above operational mode, increased RO feed salinity will result in reduced permeate productivity and decreased RO water recovery due to the rise in the feed-side osmotic pressure. Comparison of RO system performance, with and without the controller, for a set of three consecutive feed salinity pulses is shown in Figure 11, with the SEC given in Figure 12. Without control action, the RO system was set to operate at a feed pressure and a feed flow rate of 5.5 MPa and 72.7 L/min, respectively, providing permeate production of 26.9 L/min for desalting raw seawater (~33 000 mg/L TDS). Operation under control action was for the same permeate production set-point. Although in principle both the feed flow

dx.doi.org/10.1021/ie402304d | Ind. Eng. Chem. Res. 2014, 53, 7409−7420

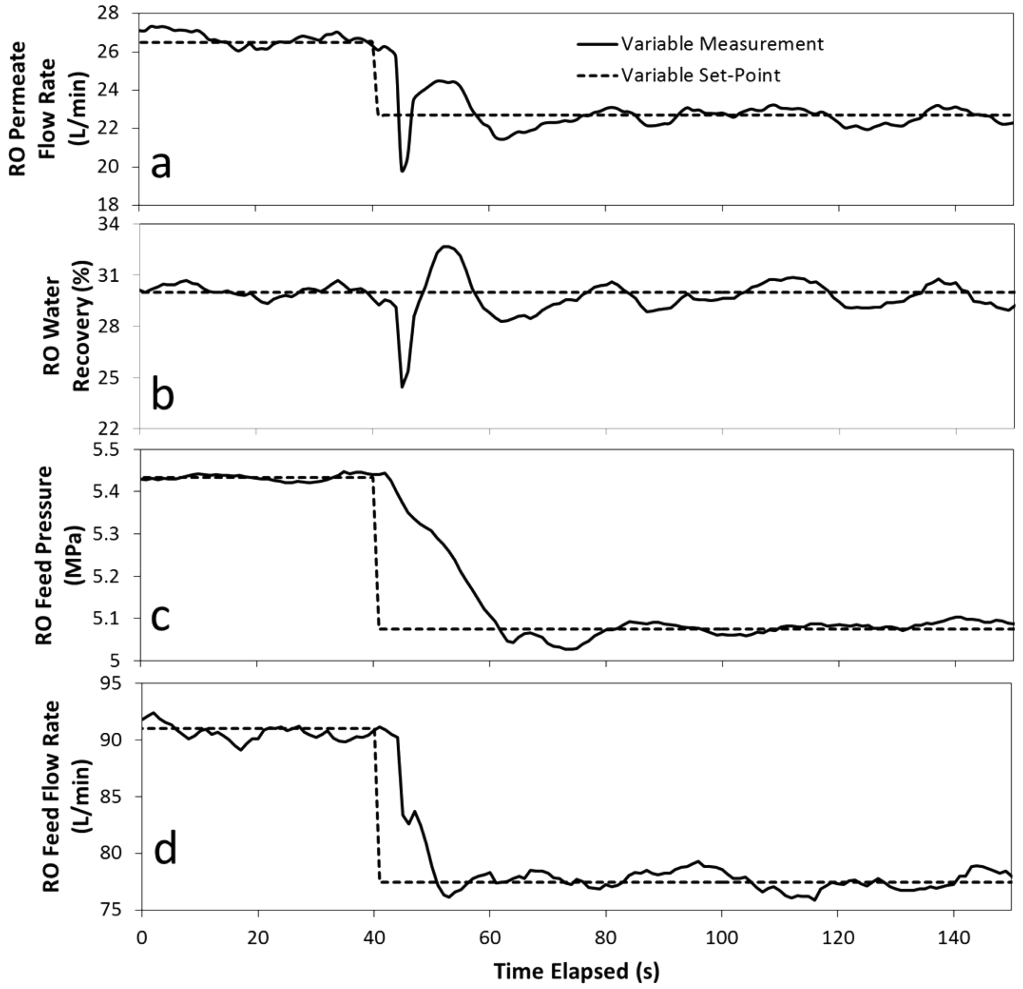

Figure 7. Profiles of (a) RO permeate flow rate, (b) RO water recovery, (c) RO feed flow rate, and (d) RO feed pressure with respect to time for a permeate flow rate set-point transition from 26.5 to 22.7 L/min. Constraints were set at $\min(Q_p) = 72.7$ L/min, $\max(P_f) = 6.9$ MPa, and $\max(Y) = 30\%$. The feed pressure set-point was changed from 5.43 to 5.07 MPa. The feed flow rate set-point was changed from 90.8 to 77 L/min.

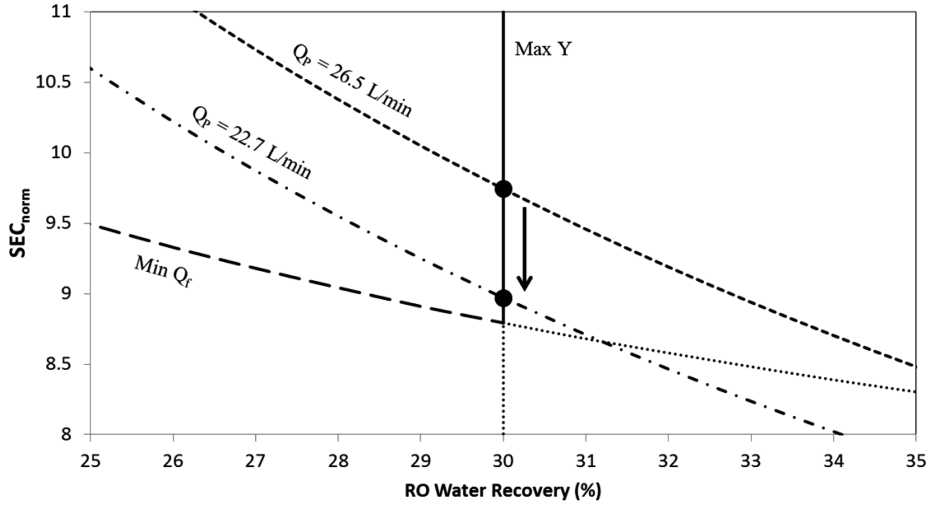

Figure 8. Normalized SEC with respect to RO recovery under the constraints $\min(Q_f) = 72.7$ L/min, $\max(P_f) = 6.9$ MPa, and $\max(Y) = 30\%$. The short dashed line is the constrained permeate flow rate curve for the initial flow rate set-point of 26.5 L/min. The dash-dotted line is the constrained permeate flow rate curve for the final flow rate set-point of 22.7 L/min. The solid circles denote the operating point of the experiment, and the arrow indicates the set-point change.

rate and pressure can be controlled for optimal operation (Section 3.4), feed pressure has the most significant impact on permeate flux. Therefore, in this test, the low-level RO controller was simplified to maintain a constant feed flow

dx.doi.org/10.1021/ie402304d | Ind. Eng. Chem. Res. 2014, 53, 7409−7420

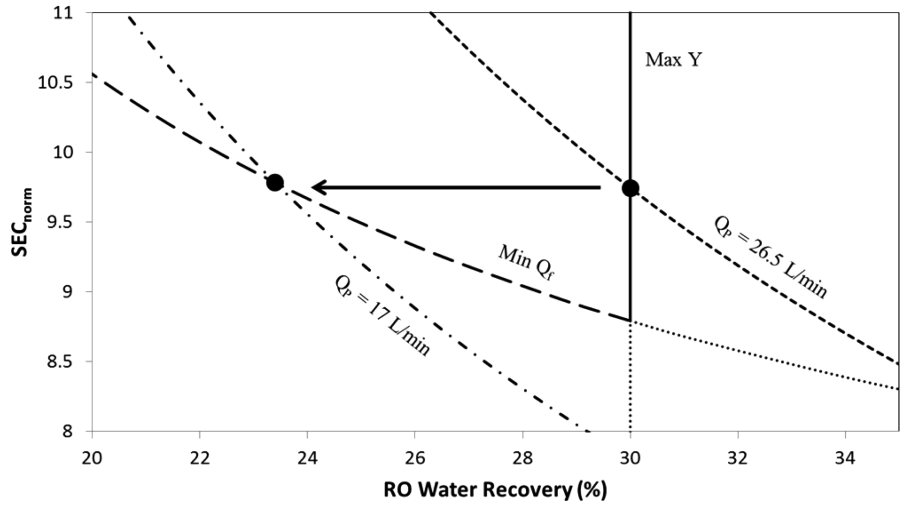

Figure 9. Normalized SEC with respect to RO recovery under constraints of min(Q_f) = 72.7 L/min, max(P_f) = 6.9 MPa, and max(Y) = 30%. The short dashed line is the constrained permeate flow rate curve for the initial flow rate set-point of 26.5 L/min. The dash-dotted line is the constrained permeate flow rate curve for the final flow rate set-point of 17 L/min. The solid circles denote the operating point of the experiment, and the arrow indicates the set-point change.

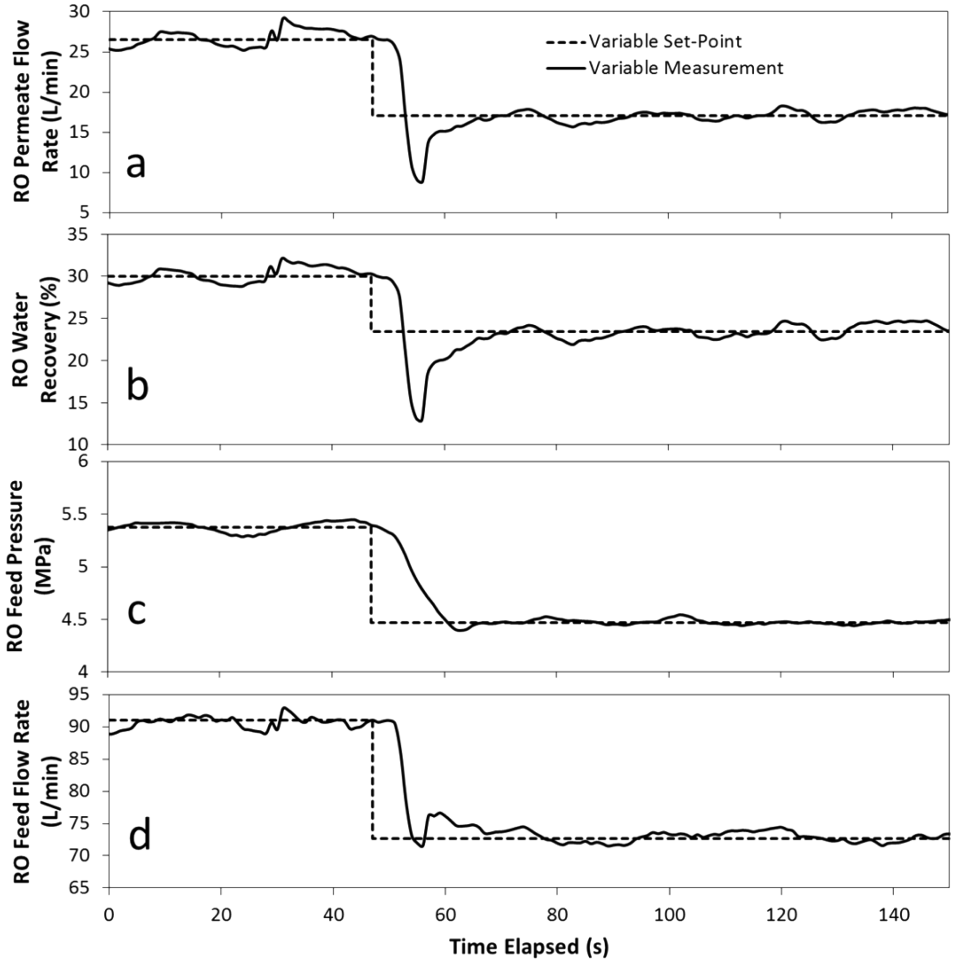

Figure 10. Profiles of (a) RO permeate flow rate, (b) RO water recovery, (c) RO feed flow rate, and (d) RO feed pressure with respect to time for a permeate flow rate set-point transition from 26.5 to 17 L/min. RO system constraints were set at min(Q_f) = 72.7 L/min, max (P_f) = 6.9 MPa, and max(Y) = 30%. Upon change in the permeate production set-point, the supervisory RO controller reduced the set-point recovery from 30% to 23.4% and changed the feed flow rate and pressure set-points from 90.8 to 72.7 L/min and from 5.38 to 4.47 MPa, respectively.

rate. However, the optimal pressure set-point was adjusted continuously (Figure 11c) in response to changing feedwater salinity (Figure 11b), as instructed by the supervisory RO controller, in order to minimize the SEC. It is apparent that

dx.doi.org/10.1021/ie402304d | Ind. Eng. Chem. Res. 2014, 53, 7409−7420

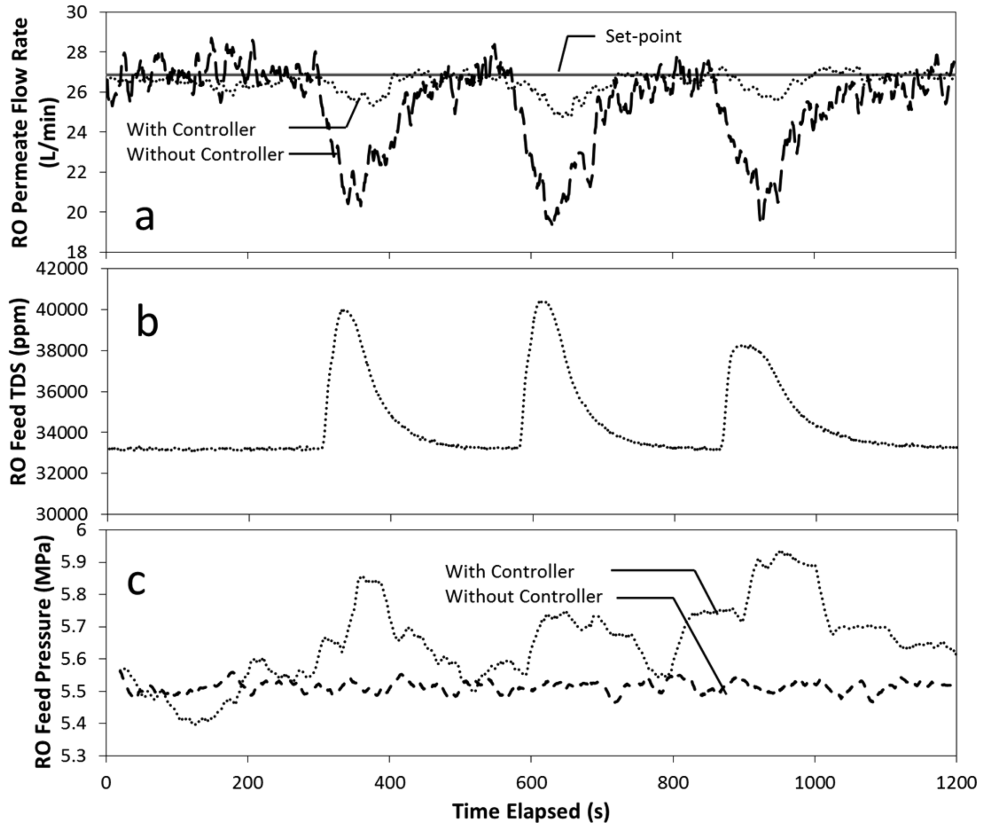

Figure 11. Profiles of the (a) RO permeate flow rate, (b) RO feed salinity, and (c) RO feed pressure with respect to time. The solid line in (c) is the permeate flow rate set-point, which is 26.9 L/min. RO system constraints were set at $\min(Q_f)$ = 72.7 L/min, $\max(P_f)$ = 6.9 MPa, and $\max(Y)$ = 30%. Plot (b) was produced using an average of both experiments because they were nearly identical.

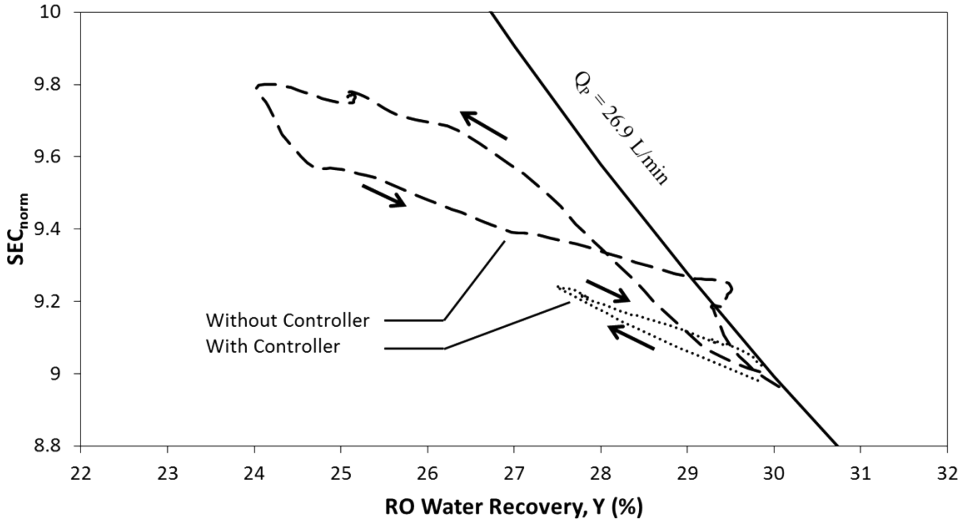

Figure 12. Normalized SEC with respect to RO recovery, with the permeate flow rate set-point over the duration of the first pulse. The solid line is the SEC curve for constant Q_p operation of 26.9 L/min. Dotted lines denote the experiment done with the controller, the dashed lines denote the experiment done without the controller, and the arrows indicate the dependence of SEC_{norm} and Y on time. Note how operation without a controller leads to a lower permeate flow rate as well as higher SEC.

without control action, permeate productivity decreased (up to 26% at the feed pulse peak salinity, Figure 11a) and SEC increased (up to 10% at the feed pulse peak salinity, Figure 12) with rising feed salinity. For example, over the duration of each of the three feed salinity pulses shown in Figure 11b, permeate productivity loss was up to about 12%. In contrast, RO operation under dynamic SEC control action, the permeate flow rate was nearer the set-point and SEC was lower (Figure 12) even when confronted with rising feed salinity. As shown in the SEC contours for plant operation during a high feed salinity pulse (Figure 12), with and without control action (dotted and dashed lines, respectively), the SEC rises with increase feed salinity as the recovery decreases but the SEC also decreases as feed salinity decreases. However, in plant operation with the

dx.doi.org/10.1021/ie402304d | Ind. Eng. Chem. Res. 2014, 53, 7409−7420

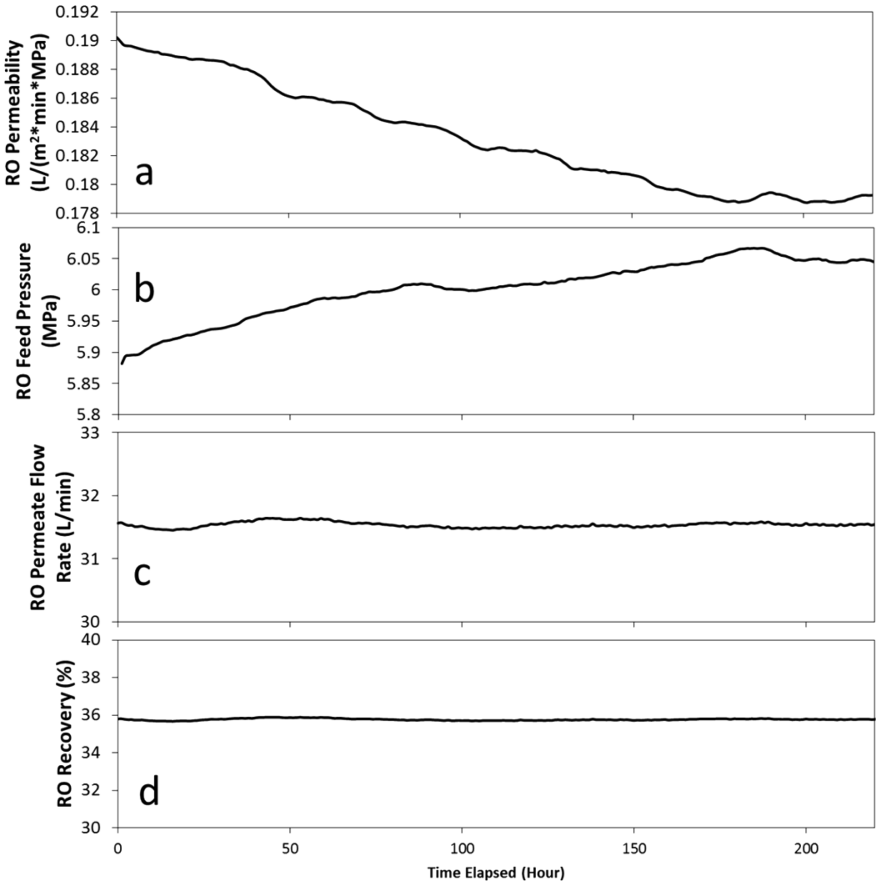

Figure 13. Profiles of RO process variables (a) membrane permeability, (b) feed pressure, (c) water recovery, and (d) permeate flux with respect to time. System constraints were set at $\min(Q_f)$ = 72.7 L/min, $\max(Y)$ = 36% and $\max(P_f)$ = 6.9 MPa, with a permeate production target of 31.4 L/min. The system set the feed flow rate at 87.2 L/min.

RO controller, the feed pressure would be continuously adjusted in response to salinity changes in order to set the recovery for operation at the lowest possible SEC.

Degradation of membrane permeability due to fouling can occur in field operations of RO desalting. As membrane permeability decreases between cleaning periods, it is desirable to maintain the desired permeate productivity while operating at a recovery that is optimal with respect to the SEC (Section 3.2). Therefore, in the present control scheme, membrane permeability is calculated (Section 3.3) and updated continuously by the supervisory RO, which is necessary for determination of the feed pressure set-point. Accordingly, as membrane permeability declines, the RO controller adjusts the feed pressure as well as feed flow rate as necessary to achieve the maximum set recovery. A demonstration of the controller's performance under RO membrane fouling conditions was carried out over a 10 day continuous RO operation with reduced feed pretreatment. As a consequence, the RO membrane fouled with a membrane permeability decline of up to 5.8% over the test period (Figure 13a). At the same time, the RO controller continuously adjusted the feed pressure upward (via control of the concentrate valve) to compensate for the decrease in permeability, whereas permeate production (Figure 13c) and recovery (Figure 13d) remained essentially constant at the desired level.

5. CONCLUSIONS

A model-based control system was implemented for the energy-optimal operation of a spiral-wound RO membrane desalination system and for maintaining system operational set-points with respect to feed pressure and flow rates (feed and permeate streams). The control scheme utilized a basic RO operational model with real-time calculations for continuous updates of membrane permeability and the feed pressure set-point. Operational control set-points were determined by a supervisory-level controller and then communicated to the lower-level controllers, which then adjusted the RO feed pressure and flow rates via control of the high pressure pump VFD and RO concentrate valve. Field tests for seawater desalination have demonstrated the controller's ability to self-adapt the system operation so as to maintain energy-optimal operation subject to constraints imposed by the system's physical components (e.g., minimum and maximum feasible or allowable flow rates and pressures) and the thermodynamic restriction for cross-flow RO operation. It was also demonstrated that the control system succeeded in maintaining both permeate production and energy-optimal operation under conditions of temporal changes in feedwater salinity. Although the present scheme was demonstrated for RO operation without an ERD, the developed control principles for energy-optimal operation is adaptable to RO system operation with ERD.

dx.doi.org/10.1021/ie402304d | Ind. Eng. Chem. Res. 2014, 53, 7409−7420

AUTHOR INFORMATION

Corresponding Authors

*P. D. Christofides. Phone: +1 (310) 794-1015. E-mail: pdc@seas.ucla.edu.

*Y. Cohen. Phone: +1 (310) 825-8766. E-mail: yoram@ucla.edu.

Notes

The authors declare no competing financial interest.

ACKNOWLEDGMENTS

This work was funded in part by the United States Office of Naval Research, the California Department of Water Resources, U.S. Bureau of Reclamation, and the UCLA Water Technology Research Center. The authors acknowledge the contributions of Dr. Richard Zhu on the initial design of the control system and of Dr. Alex Bartman on the software implementation of the control system. The assistance of John Thompson in the construction of the pilot system is also acknowledged. The authors also acknowledge support by Danfoss Sea Recovery (Henrik Wendelboe and Christopher Okada), Inge GmbH (Peter Berg, Martin Heijnen, and Josef Wunram), Georg Fischer (Rick Hines), and Dow Water & Process Solutions (Michael Kim) and Ahlstrom (Rod Komlenic and Denise Russell) for equipment contributions toward construction of the desalination plant. The personnel of the Seawater Desalination Test Facility at the U.S. Naval Base Ventura County (William Varnava, Mark Miller, Paul Giuffrida, and Micah Ing) are also acknowledged for their technical assistance during the field study.

REFERENCES

(1) Gray, S.; Semiat, R.; Duke, M.; Rahardianto, A.; Cohen, Y. Seawater Use and Desalination Technology. In *Treatise on Water Science*; Peter, W., Ed.; Elsevier: Oxford, U.K., 2011; pp 73−109.

(2) Fethi, K. Optimization of energy consumption in the 3300 m^3/d RO Kerkennah plant. *Desalination* **2003**, *157* (1−3), 145−149.

(3) Nemeth, J. E. Innovative system designs to optimize performance of ultra-low pressure reverse osmosis membranes. *Desalination* **1998**, *118* (1−3), 63−71.

(4) Wilf, M. Design consequences of recent improvements in membrane performance. *Desalination* **1997**, *113* (2−3), 157−163.

(5) Oklejas, E., Jr; Pergande, W. F. Integration of advanced high-pressure pumps and energy recovery equipment yields reduced capital and operating costs of seawater RO systems. *Desalination* **2000**, *127* (2), 181−188.

(6) Rautenbach, R.; Dahm, W. Design and Optimization of Spiral-Wound and Hollow Fiber Ro-Modules. *Desalination* **1987**, *65* (1−3), 259−275.

(7) Avlonitis, S.; Hanbury, W. T.; Benboudinar, M. Spiral Wound Modules Performance - an Analytical Solution 0.1. *Desalination* **1991**, *81* (1−3), 191−208.

(8) Boudinar, M. B.; Hanbury, W. T.; Avlonitis, S. Numerical simulation and optimization of spiral-wound modules. *Desalination* **1992**, *86* (3), 273−290.

(9) Avlonitis, S.; Hanbury, W. T.; Benboudinar, M. Spiral Wound Modules Performance - an Analytical Solution 0.2. *Desalination* **1993**, *89* (3), 227−246.

(10) van der Meer, W. G. J.; van Dijk, J. C. Theoretical optimization of spiral-wound and capillary nanofiltration modules. *Desalination* **1997**, *113* (2−3), 129−146.

(11) Geraldes, V.; Pereira, N. E.; de Pinho, M. N. Simulation and optimization of medium-sized seawater reverse osmosis processes with spiral-wound modules. *Ind. Eng. Chem. Res.* **2005**, *44* (6), 1897−1905.

(12) Villafafila, A.; Mujtaba, I. M. Fresh water by reverse osmosis based desalination: simulation and optimization. *Desalination* **2003**, *155* (1), 1−13.

(13) Avlonitis, S. A.; Pappas, M.; Moutesidis, K. A unified model for the detailed investigation of membrane modules and RO plants performance. *Desalination* **2007**, *203* (1−3), 218−228.

(14) Singh, R.; Cabibbo, S. V. Hydraulic turbine energy recovery - R.O. System. *Desalination* **1980**, *32*, 281−296.

(15) Woodcock, D. J.; White, I. M. The application of pelton type impulse turbines for energy recovery on sea water reverse osmosis systems. *Desalination* **1981**, *39*, 447−458.

(16) El-ghonemy, A. M. K. Waste energy recovery in seawater reverse osmosis desalination plants. Part 1: Review. *Renewable Sustainable Energy Rev.* **2013**, *18*, 6−22.

(17) Bartels, C. R.; Andes, K. Consideration of energy savings in SWRO. *Desalin. Water Treat.* **2013**, *51* (4−6), 717−725.

(18) Kim, Y.; Kang, M. G.; Lee, S.; Jeon, S. G.; Choi, J. S. Reduction of energy consumption in seawater reverse osmosis desalination pilot plant by using energy recovery devices. *Desalin. Water Treat.* **2013**, *51* (4−6), 766−771.

(19) Geisler, P.; Hahnenstein, F. U.; Krumm, W.; Peters, T. Pressure exchange system for energy recovery in reverse osmosis plants. *Desalination* **1999**, *122* (2−3), 151−156.

(20) Lu, Y.-Y.; Hu, Y.-D.; Zhang, X.-L.; Wu, L.-Y.; Liu, Q.-Z. Optimum design of reverse osmosis system under different feed concentration and product specification. *J. Membr. Sci.* **2007**, *287* (2), 219−229.

(21) Manth, T.; Gabor, M.; Oklejas, E. Minimizing RO energy consumption under variable conditions of operation. *Desalination* **2003**, *157* (1−3), 9−21.

(22) Busch, M.; Mickols, W. E. Reducing energy consumption in seawater desalination. *Desalination* **2004**, *165* (1−3), 299−312.

(23) Wilf, M.; Klinko, K. Optimization of seawater RO systems design. *Desalination* **2001**, *138* (1−3), 299−306.

(24) Wilf, M.; Bartels, C. Optimization of seawater RO systems design. *Desalination* **2005**, *173* (1), 1−12.

(25) Alatiqi, I.; Ettouney, H.; El-Dessouky, H. Process control in water desalination industry: an overview. *Desalination* **1999**, *126* (1−3), 15−32.

(26) Alatiqi, I. M.; Ghabris, A. H.; Ebrahim, S. System-Identification and Control of Reverse-Osmosis Desalination. *Desalination* **1989**, *75* (1−3), 119−140.

(27) Bartman, A. R.; Christofides, P. D.; Cohen, Y. Nonlinear Model-Based Control of an Experimental Reverse-Osmosis Water Desalination System. *Ind. Eng. Chem. Res.* **2009**, *48* (13), 6126−6136.

(28) McFall, C. W.; Bartman, A.; Christofides, P. D.; Cohen, Y. Control and monitoring of a high recovery reverse osmosis desalination process. *Ind. Eng. Chem. Res.* **2008**, *47* (17), 6698−6710.

(29) Abbas, A. Model predictive control of a reverse osmosis desalination unit. *Desalination* **2006**, *194* (1−3), 268−280.

(30) Bartman, A. R.; McFall, C. W.; Christofides, P. D.; Cohen, Y. Model-predictive control of feed flow reversal in a reverse osmosis desalination process. *J. Process. Control* **2009**, *19* (3), 433−442.

(31) Gambier, A.; Badreddin, E. Application of hybrid modeling and control techniques to desalination plants. *Desalination* **2003**, *152* (1−3), 175−184.

(32) Krstic, M. Performance improvement and limitations in extremum seeking control. *Syst. Control Lett.* **2000**, *39* (5), 313−326.

(33) Bartman, A. R.; Zhu, A. H.; Christofides, P. D.; Cohen, Y. Minimizing energy consumption in reverse osmosis membrane desalination using optimization-based control. *J. Process Control* **2010**, *20* (10), 1261−1269.

(34) Zhu, A. Z.; Christofides, P. D.; Cohen, Y. Effect of Thermodynamic Restriction on Energy Cost Optimization of RO Membrane Water Desalination. *Ind. Eng. Chem. Res.* **2009**, *48* (13), 6010−6021.

(35) Zhu, A. H.; Christofides, P. D.; Cohen, Y. Minimization of energy consumption for a two-pass membrane desalination: Effect of

energy recovery, membrane rejection and retentate recycling. *J. Membr. Sci.* **2009**, *339* (1−2), 126−137.
(36) Zhu, A. H.; Rahardianto, A.; Christofides, P. D.; Cohen, Y. Reverse osmosis desalination with high permeability membranes - Cost optimization and research needs. *Desalin. Water Treat.* **2010**, *15* (1−3), 256−266.
(37) Zhu, A. H.; Christofides, P. D.; Cohen, Y. Energy Consumption Optimization of Reverse Osmosis Membrane Water Desalination Subject to Feed Salinity Fluctuation. *Ind. Eng. Chem. Res.* **2009**, *48* (21), 9581−9589.
(38) Mulder, M. *Basic Principles of Membrane Technology*; Kluwer Academic Publishers: Boston, MA, 1997.
(39) Dow Water & Process Solutions, *FILMTEC Membranes—System Design, System Performance Projection (Form No. 609-00071-1009)*; Dow Chemical Company: Midland, MI; pp. 89−92. http://msdssearch.dow.com/PublishedLiteratureDOWCOM/dh_0036/0901b803800362e9.pdf?filepath=liquidseps/pdfs/noreg/609-02057.pdf&fromPage=GetDoc (accessed Aug 22, 2013).